analytical chemistry

pubs.acs.org/ac Article

An Ultrasensitive Electrochemical Biosensor Integrated by Nicking Endonuclease-Assisted Primer Exchange Reaction Cascade Amplification and DNA Nanosphere-Mediated Electrochemical Signal-Enhanced System for MicroRNA Detection

Sha Yu,[§] Siyu Chen,[§] Yuan Dang, Yuanzhen Zhou,* and Jun-Jie Zhu*

Cite This: *Anal. Chem.* 2022, 94, 14349−14357 Read Online

ACCESS | Metrics & More | Article Recommendations | Supporting Information

ABSTRACT: Specific and sensitive microRNAs (miRNAs) detection is essential to early cancer diagnosis. The development of these technologies including functional nuclease-mediated target amplification and DNA nanotechnology possesses tremendous potential for the high-performance detection of miRNAs in the accurate diagnosis of disease. In this study, we have established an ultrasensitive electrochemical biosensor by combining nicking endonuclease-assisted primer exchange reaction (PER) cascade amplification with a DNA nanosphere (DNS)-mediated electrochemical signal-enhanced system for the detection of miRNA-21 (miR-21). The cascade amplification is initiated by a nicking endonuclease that can cleave specific DNA substrates and highly amplify translation of the target to single-stranded DNA fragments (sDNA). Then, the PER cascade is powered by strand-displacing polymerase and generates a large amount of nascent single-stranded connector DNA (cDNA) via sDNA triggering of the dumbbell probe (DP), thus achieving the cascade amplification of the target. Finally, the DNS loaded with plenty of electroactive substances can be captured on the electrode via cDNA for further enhancing the electrochemical signal and highly sensitive detection of miR-21. The proposed electrochemical biosensor exhibits a wide detection range of 1 aM to 0.1 nM and a low detection limit of 0.58 aM. The excellent selectivity allows the biosensor to discriminate miR-21 from other miRNAs, even the one base-mismatched sequence. Moreover, the practicability of the biosensor is investigated by analyzing miR-21 in human serum and cancer cell lysate. Therefore, our proposed nicking endonuclease-assisted PER cascade amplification strategy provides a powerful platform for the early detection of miRNA-related disease and molecular diagnosis.

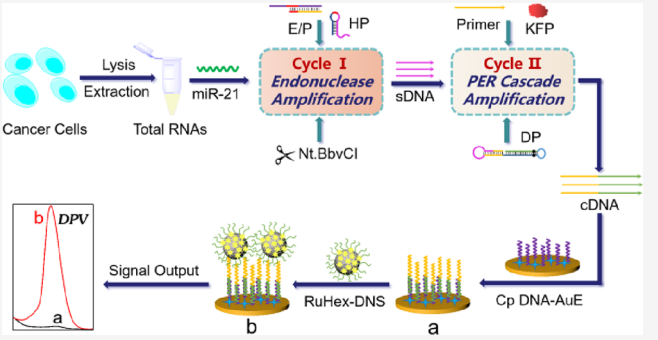

Downloaded via TSINGHUA UNIV on November 9, 2022 at 13:26:35 (UTC).
See https://pubs.acs.org/sharingguidelines for options on how to legitimately share published articles.

INTRODUCTION

MicroRNAs (miRNAs) are a class of short noncoding single-stranded RNAs that play important roles in physiological activities, such as gene regulation,[1] cell differentiation,[2] cell proliferation, and apoptosis.[3] Moreover, numerous studies have shown that miRNAs are closely associated with the progression of various diseases, such as cancers,[4] heart diseases,[5] and diabetes.[6] Therefore, miRNAs are discussed as promising biomarker candidates and their accurate detection is of great significance not only for dynamic monitoring of human physiological activity but also for early diagnosis and intervention in related diseases. Northern blotting, microarray technology, and real-time polymerase chain reaction (qT-PCR) are traditional analytical methods for identification and quantification of miRNAs.[7−9] However, the inherent characteristics of miRNAs, including low abundance, high sequence homology, and easy degradability,[10] rendering the sensitivity and specificity of these methods are not amenable for miRNAs detection. In addition, the sophisticated operations, time-consuming property, and requirement for plenty of samples largely limit the further practical applications of these methods as well.[11,12]

To break these limits, a series of molecule signal amplification methods, especially the nuclease-assisted signal amplification techniques, for instance, rolling circle amplification (RCA),[13] polymerization/nicking reaction (PNR),[14] and loop-mediated isothermal amplification (LAMP),[15] that can achieve simple, fast, and efficient amplification of the target miRNAs have been developed. However, these nuclease-driven

Received: July 13, 2022
Accepted: September 20, 2022
Published: October 3, 2022

© 2022 American Chemical Society

https://doi.org/10.1021/acs.analchem.2c03015
Anal. Chem. 2022, 94, 14349−14357

amplification systems always require complex primer design and involve multiple nucleases.[16,17] In addition, the amplification efficiency and stability are also limited by nuclease activity.[18] All of these factors greatly affect the stability of target amplification. Alternatively, the primer exchange reaction (PER) cascade strategy as an emerging technology has been proposed for amplification of the target in recent years. The PER cascade uses a catalytic DNA hairpin (named as PER hairpin) as a template, and the short single-stranded DNA (ssDNA) primer can continually grow nascent ssDNA according to the prescribed reaction pathways with the help of the strand-displacing polymerase to achieve the stable amplification of target sequences.[19,20] More importantly, only when the right set of PER hairpin and the corresponding PER primer coexist is a new strand produced autonomously in situ,[21] which makes little signal leakage and thus effectively reduces the reaction background. Inspired by this specific reaction, the PER cascade has been extensively applied to highly sensitive detection of miRNAs by colorimetric,[22] fluorescent,[23] and electrochemical technologies.[24] Among them, the electrochemistry-based detection methods, especially the label-free strategies, have increasingly attracted attention due to the advantages of simplicity, speediness, high sensitivity, and repeatability.[25,26] Considering the unique characteristics of miRNAs, it is still a great challenge of combining diverse nuclease-assisted target amplification techniques in series for the multiple amplification and highly sensitive electrochemical detection of miRNAs.

On the other hand, the electrochemical signal output intensity is always limited by the effective area of the working electrode. Therefore, the development of high-throughput signal molecule carriers on the electrode interface is also an important idea to improve the sensitivity of electrochemical detection. To fundamentally overcome the limitations of the two-dimensional electrode interface, many research studies have demonstrated that using the three-dimensional porous nanomaterials, such as covalent organic frameworks (COFs),[27] metal organic frameworks (MOFs),[28] and mesoporous silica nanoparticles (MSNs),[29] as the electroactive substance carriers can effectively improve the electrochemical signal intensity so as to achieve highly sensitive detection of the low abundance targets. Unfortunately, these nanomaterials are still challenged by lack of recognition ability for targets, poor stability, sophisticated preparation and functionalization processes.[30,31] In contrast, the three-dimensional DNA nanostructures, including DNA polyhedrons,[32] DNA dendrimers,[33] DNA nanoflowers,[34] and DNA nanospheres,[35] constructed through the simple DNA self-assembly have been used as nanocarriers and widely applied in the field of biosensing, biomedicine, and drug delivery. Moreover, the unique Watson−Crick base-pairing endows these nanocarriers with excellent specificity and robust stability in complex body liquid.[36] Particularly, their large surface areas will offer abundant binding sites for small molecules.[37] Taken together, we believe that these DNA nanostructures will be promising carriers that can easily imbed lots of electroactive substances for maintaining the electrochemical signal output with high intensity and steadiness.

Herein, we have constructed a nuclease-assisted cascade amplification strategy by integrating nicking endonuclease-assisted target amplification with a PER cascade while using the DNA nanospheres (DNS) as signal molecule carriers for the improvement of the electrochemical signal intensity, eventually achieving the sensitively and specifically electrochemical detection of miRNA-21 (miR-21). Furthermore, by analyzing miR-21 in human serum and its expression level in different cell lines, this biosensor practicability in real sample analysis and accurate cancer diagnosis has been verified.

EXPERIMENTAL SECTION

Nicking Endonuclease-Assisted PER Cascade Amplification Strategy. For the nicking endonuclease-assisted target amplification, the amount of Nt.BbvCI and reaction time were optimized as 0.2 U/μL and 2 h, respectively (see Figure S3, Supporting Information). Briefly, the 24.5 μL reaction system, including 1 μL of miR-21 (1 fM), 5 μL of pre-annealed hairpin DNA (HP, 1 nM), 5 μL of enzyme substrate strand (E, 1 nM), 7.5 μL of protecting strand (P, 1 nM), 1 μL of Nt.BbvCI (0.2 U/μL), and 5 μL of rCutSmart (1×), was first mixed at 4 °C. After incubating at 37 °C for 2 h, the mixture was subsequently kept at 80 °C for 20 min to inactivate Nt.BbvCI and then cooled naturally to room temperature to obtain the single-stranded DNA fragments (sDNA) generated from the cleaving of E by Nt.BbvCI, which could trigger the next PER cascade. The amount of Klenow(exo) fragment polymerase (KFP) used in the PER cascade and reaction time were first optimized as 0.05 U/μL and 2 h, respectively (see Figure S3, Supporting Information). Specifically, 5 μL of pre-annealed dumbbell probe (DP, 1 nM), 5 μL of Prime (10 nM), 5 μL of dNTP (100 nM), 0.5 μL of KFP, (0.05 U/μL), 5 μL of NEbuffer2 (1×), and 5 μL of ultrapure water were successively mixed with the nicking endonuclease-assisted reaction system. After incubation at 37 °C for 2 h, KFP was completely inactivated at 75 °C for 20 min and then the mixture was cooled naturally to room temperature. The resultant products of nicking endonuclease-assisted target amplification and PER cascade were analyzed by 12% native polyacrylamide gel electrophoresis (PAGE) in 1× TBE solution consisting of Tris (40 mM), acetic acid (20 mM), and EDTA (1 mM, pH 7.4) at 150 V for 40 min. After staining and water elution, the resulting gel was imaged by a BIO-RAD ChemiDoc XRS.

Preparation of DNS. DNS were prepared according to the literature.[35] The preparation of DNS used "Y-shaped" DNA as the structural unit. In detail, the probes of H1, H2, and H3 were first separately annealed at 95 °C for 5 min and slowly cooled to room temperature to obtain the desired secondary structure. Then, H1 (10 μM) and H2 (10 μM) were mixed in TE buffer and incubated at 37 °C for 4 h to form DNA dimers. Finally, the same volumes of H3 (10 μM) and I (5 μM) were added into the above mixture and incubated at 37 °C for another 4 h to obtain the DNS, which could load a mass of electroactive substances to improve the electrochemical signal intensity.

Electrochemical Detection of miR-21. First, the 4 mm-diameter gold electrode (AuE) was immersed in piranha solution (a mixture of 98% H_2SO_4 and 30% H_2O_2 at 3:1 volume ratio) for 30 min and thoroughly rinsed with ultrapure water. The electrodes were then successively polished with 0.3 and 0.05 μm alumina for 3 min to obtain a mirror surface. Subsequently, these electrodes were cleaned with ethanol and ultrapure water for 5 min to remove the residual alumina powder and then electrochemically cleaned by continuous scanning between −0.2 and +1.6 V at a scanning rate of 0.1 V/s in the newly configured H_2SO_4 (0.5 M) until stable cyclic voltammetry (CV) was obtained. Finally, these electrodes were cleaned with RNase-free water and dried with nitrogen for later use.

https://doi.org/10.1021/acs.analchem.2c03015
Anal. Chem. 2022, 94, 14349−14357

Scheme 1. Schematic Illustration of the Electrochemical Biosensor for Ultrasensitive Detection of miR-21[a]

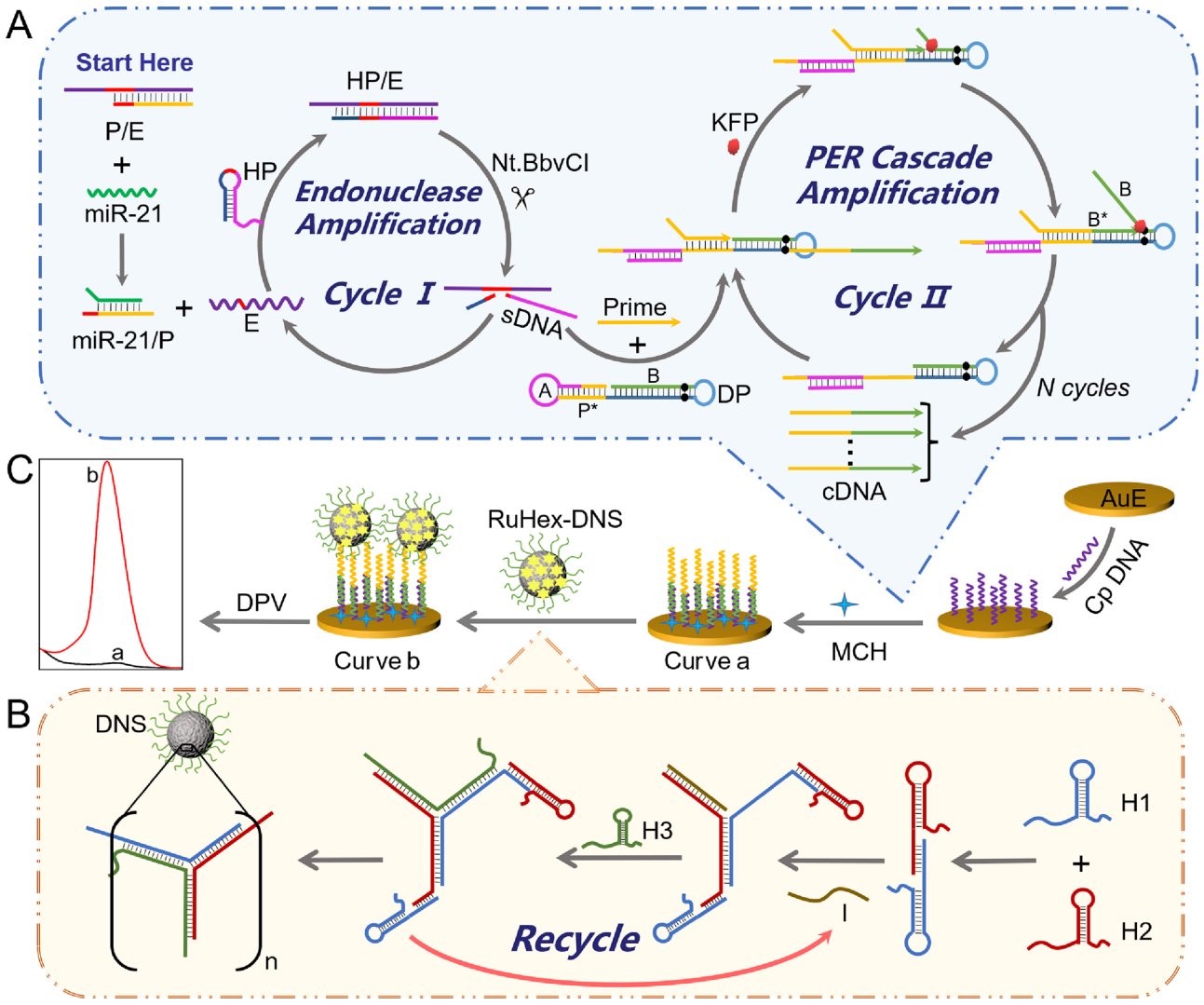

[a](A) Diagram of nicking endonuclease-assisted target recycling (cycle I) and PER cascade (cycle II); (B) assembly procedure of DNS; (C) electrochemical detection of miR-21.

For the gold electrode modification, 10 μL of thiol-labeled capture DNA (Cp DNA, 1 μM) pretreated with tris(2-carboxyethyl)phosphine (TCEP, 10 mM, pH 5.2) for 1 h was dropped on the surface of the pretreated gold electrode at room temperature, incubated overnight at 4 °C (~16 h), and then incubated for 2 h at 37 °C to obtain the Cp DNA-modified gold electrode (Cp DNA-AuE). The resulting electrodes were washed twice with ultrapure water and subsequently immersed into 6-mercapto-1-hexanol (MCH, 1 mM) at room temperature for 1 h to seal the redundant active sites of the gold electrode. After washing these electrodes twice with ultrapure water, 5 μL of the product obtained from the nuclease-assisted target cascade amplification reaction was dropped onto these electrodes and incubated at 37 °C for 2 h before cleaning twice. Then, 10 μL of DNS loaded with $[Ru(NH_3)_6]^{3+}$ (RuHex) was dropped on the gold electrode and incubated at 37 °C for 2 h before cleaning twice for later use. Differential pulse voltammetry (DPV) tests were performed in Tris−HCl (10 mM, pH 7.4) deoxidized with nitrogen in the scanning interval of +0.4 to −0.6 V (vs SCE).

RESULTS AND DISCUSSION

Principle of the Nicking Endonuclease-Assisted PER Cascade Amplification Strategy. The proposed electrochemical biosensor mainly includes two amplification processes: (1) nicking endonuclease-assisted target amplification; (2) strand-displacing polymerase-assisted PER cascade (Scheme 1A). In this design, miR-21, an important biomarker of various human malignancies,[38] is taken as the target. The enzyme substrate strand (E) containing the nicking endonuclease cleavage recognition region is prehybridized with the protection strand (P) to form the P/E hybrid. In the presence of miR-21, the E strand can be released by toehold-mediated strand displacement (TMSD) reactions accompanied by the formation of a miR-21/P hybrid. Then, the released E strand unfolds the hairpin DNA (HP), which can activate the nicking endonuclease, leading to the HP cleavage and generation of single-stranded DNA fragments (sDNA), whereas the released E strand is recycled to hybridize with another HP and initiate a new nicking endonuclease cleavage cycle. Thus, one miR-21 can cause numerous HP cleavage powered by nicking endonuclease, leading to the target continuous amplification

https://doi.org/10.1021/acs.analchem.2c03015
Anal. Chem. 2022, 94, 14349−14357

(cycle I). Then, a dumbbell probe (DP) with two loops is designed to execute the PER cascade. One loop (domain A) can be opened by sDNA and expose domain P* to hybridize with the Primer. Subsequently, the Primer can be extended by copying domain B (termed as the copy region of the PER hairpin) before halting at the stop sequence on the PER hairpin with the aid of strand-displacing polymerase (KFP). The copied domain B* is then able to compete with B on the PER hairpin via the random walk process of three-way branch migration. Finally, the extended Primer, a nascent single-stranded connector DNA (that is Primer+B*, named as cDNA) can spontaneously dissociate from the PER hairpin once the copied domain B has been displaced. Meanwhile, the free PER hairpin can immediately bind with another Primer to induce a new PER cycle. Thus, the sDNA-initiated PER cascade can generate a large amount of cDNA for further amplification of the transcription fragment of the target (cycle II). For electrochemical detection, the DNA nanospheres (DNS) with an abundant DNA double helix structure can absorb lots of electroactive substances, such as RuHex, which thus can be used as the signal molecule carrier for the enhancement of the electrochemical signal (RuHex-DNS). The self-assembly process of DNS is displayed in Scheme 1B, and the specific description is shown in the Supporting Information. From Scheme 1C, when RuHex-DNS is captured on the gold electrode via the complementation between capture DNA (Cp DNA) and cDNA, a remarkably amplified electrochemical DPV signal can be observed for quantitative detection of miR-21 (curve b). In the absence of miR-21, the nicking endonuclease-assisted PER cascade amplification reaction is inactive and RuHex-DNS cannot be captured on the electrode, thus, only a very weak DPV signal is detected (curve a). The proposed electrochemical biosensing platform integrating both the nicking endonuclease-assisted PER cascade amplification strategy and DNS-mediated electrochemical signal-enhanced system holds great potential in highly sensitive determination of miRNAs.

Native Polyacrylamide Gel Electrophoretic Characterization. The reaction pathways of the nicking endonuclease-assisted PER cascade amplification strategy are investigated by native PAGE. For the nicking endonuclease-assisted target amplification (Figure 1A), lanes 1, 2, 3, and 4 with a clear single band corresponded to HP, E, miR-21, and P, respectively, which were used as the control. The E/HP hybrid (lane 5), E/P hybrid (lane 6), and P/miR-21 hybrid (lane 7) exhibited new high molecular weight bands, indicating that these DNAs have been hybridized successfully. In the absence of miR-21, the E/HP hybrid that could activate the nicking endonuclease has not appeared (lane 8), indicating that the P strand could effectively seal the E strand, thus reducing the background signal. In contrast, after incubating with miR-21, the E/HP hybrid was generated (lane 9), which could be cleaved to release sDNA and intact E strand simultaneously upon further incubation with nicking endonuclease (lane 10). All of these results indicate that the enzyme cleavage reaction can be triggered only in the presence of miR-21.

For the strand-displacing polymerase-assisted PER cascade (Figure 1B), a clear single band appeared in lanes 1, 2, and 10, corresponding to DP, sDNA, and cDNA, respectively. No obvious band appeared in lane 3 because the sequence is too short to stain with GelRed. When sDNA and DP coexisted, there was an obvious high molecular weight band corresponding to the sDNA/DP hybrid (lane 4), indicating that sDNA

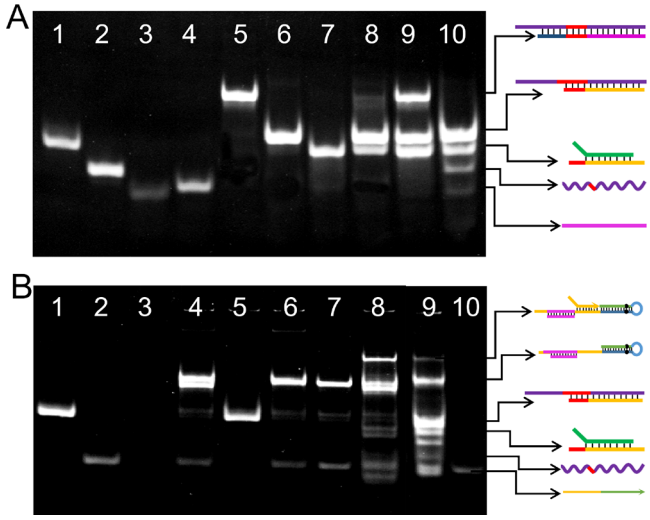

Figure 1. Native PAGE characterized the feasibility of the designed cascade amplification strategy: (A) lane 1, HP; lane 2, E; lane 3, miR-21; lane 4, P; lane 5, HP/E; lane 6, E/P; lane 7, miR-21/P; lane 8, E/P + HP; lane 9, E/P + HP + miR-21; lane 10, E/P + HP + miR-21 + Nt.BbvCI. (B) lane 1, DP; lane 2, sDNA; lane 3, Prime; lane 4, DP + sDNA + KFP + dNTP; lane 5, DP + Prime + KFP + dNTP; lane 6, DP + sDNA + Prime + KFP; lane 7, DP + sDNA + Prime + dNTP; lane 8, DP + sDNA + Prime + KFP + dNTP; lane 9, nicking endonuclease-assisted target amplification + lane 7; lane 10, cDNA.

could successfully open the DP. When all the reactive species were present (including dNTP, KFP, Prime, DP, and sDNA), an obvious cDNA band appeared (lane 8). Whereas, in the absence of one species, no cDNA bands could be observed (lanes 4, 5, 6, and 7). Furthermore, when the nicking endonuclease-assisted target amplification was combined with the PER cascade, a brighter cDNA band was yielded (band 9), which demonstrates that the proposed cascade amplification strategy has a significant target amplification effect.

Characterization of DNS. The self-assembly pathway of DNS is first confirmed by native PAGE. As shown in Figure 2A, the three types of hairpin DNAs (H1, H2, and H3) and initiation strand (I) were used as controls (lanes 1, 2, 3, and 4, respectively). After incubation of H1 and H2, a new band appeared (lane 5), indicating that the H1/H2 dimer successfully formed. When the mixture was incubated with I, a higher molecular weight band occurred in lane 6, demonstrating that a higher-order H1/H2 dimer could be formed triggered by I. With the addition of H3, two obvious new bands were produced (lane 7), one is the "Y"-shaped assembly unit, which can further self-assemble and eventually form a new DNA nanostructure with a high molecular weight, that is DNS. Moreover, the morphology of DNS was characterized by TEM, a large number of uniformly dispersed spherical structures were observed in Figure 2B, and the size was statistically analyzed as 29 nm (Figure S2), further verifying the successful preparation of DNS.

Characterization of Fabricated Electrodes. Electrochemical impedance spectroscopy (EIS), which can reflect the electron transfer resistance via the diameter of the semicircle domain,[39] is first implemented to monitor the fabrication pathways of the electrochemical biosensor (Figure 3A). The bare gold electrode with an excellent electron transfer rate displayed an extremely narrow semicircle in the impedance spectrum (curve a). After being modified with Cp DNA, an

https://doi.org/10.1021/acs.analchem.2c03015
Anal. Chem. 2022, 94, 14349−14357

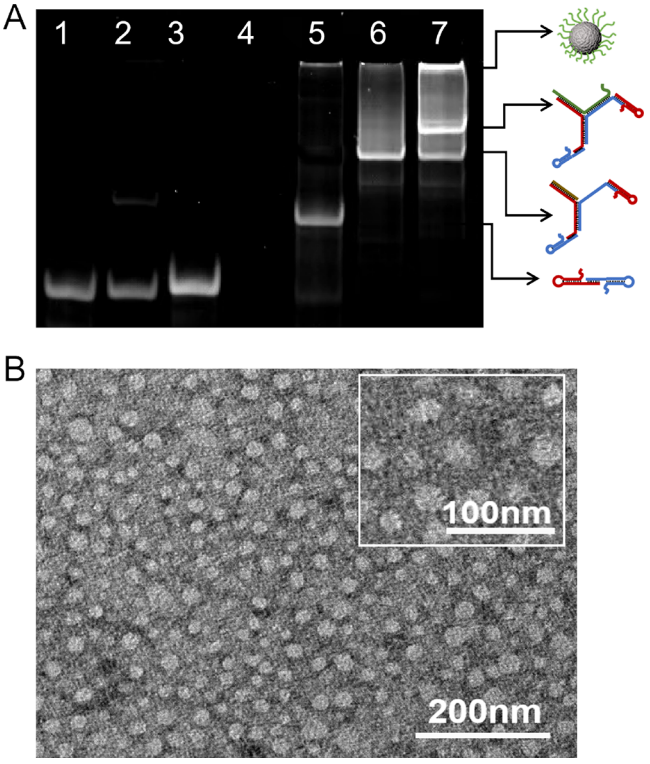

Figure 2. Characterization of DNS. (A) Native PAGE characterized the preparation process of DNS. lane 1, H1; lane 2, H2; lane 3, H3; lane 4, I (the short single-stranded I does not stain with GelRed); lane 5, H1 + H2; lane 6, H1 + H2 + I; lane 7, H1 + H2 + I + H3. (B) TEM image of DNS.

enlarged semicircle was observed due to the repulsion between the negatively charged DNA and $[Fe(CN)_6]^{3-/4-}$ (curve b).[40] Then, the charge transfer resistance gradually increased with the increase in diameter, which was observed after treatment with MCH (curve c) and obtaining cDNA from the nicking endonuclease-assisted PER cascade amplification strategy (curve d) successively. Remarkably, upon further incubation with DNS, the electrochemical impedance increased significantly (curve e), which was attributed to the repulsion of a large amount of negatively charged DNA network skeletons inside the DNS and $[Fe(CN)_6]^{3-/4-}$.

Subsequently, DPV is further used to investigate the feasibility of the fabricated electrochemical biosensor. RuHex with an electrochemical response can be absorbed to the anionic phosphate of DNA via electrostatic interaction,[41] thus, RuHex is used as a signal reporter molecule to indicate the level of miR-21 in this study. From Figure 3B, the bare gold electrode had almost no DPV signal (curve a), and a very weak DPV signal was observed on the Cp DNA-modified electrode (curve b). In contrast, after incubation with cDNA obtained from nicking endonuclease-assisted target amplification (cycle I, curve c) and PER cascades (cycle II, curve d), the DPV intensity was slightly increased and the signal intensity of cycle II was higher than that of cycle I, indicating that more cDNA can be obtained by PER cascades. When incubated with the cDNA generated by the nicking endonuclease-assisted PER cascade amplification strategy (cycle I + cycle II), the increased DPV signal was recorded (curve e), indicating that this nuclease-assisted target cascade amplification strategy has excellent signal amplification efficiency. To further improve the electrochemical signal intensity, RuHex-DNS was captured on the gold electrode via cDNA and resulted in a significantly enhanced electrochemical signal (curve f).

It has been reported that the signal-to-noise (S/N) ratio can well reflect the performance of the constructed biosensor, especially for the molecular signal amplification technology.[42,43] To obtain better sensitivity, the S/N ratio and signal amplification factor (that is the ratio of electrochemical signal with and without the amplification strategy) of the electrochemical biosensor constructed by different amplification strategies used in this study are further explored (Figure 3C). Obviously, cycle I + cycle II held the highest S/N ratio (the red line) and amplification factor (the black line), indicating that this biosensor has an excellent S/N ratio and a high signal amplification efficiency, which ensures the sensitivity of the established electrochemical biosensor. In addition, it has been demonstrated that cycle I + cycle II always maintained the highest signal intensity, even if the reaction time was extended (Figure S4), further verifying that the proposed nicking endonuclease-assisted PER cascade amplification strategy has excellent signal amplification performance. Furthermore, in comparison with the DNS that was directly assembled on the electrode (method a), a larger DPV peak current response with excellent stability was observed when the DNS was first assembled in buffer solution and then captured on the electrode via cDNA (method b) (Figure 3D and Figure S5), thus, this method was used in the subsequent electrochemical assays. All of these results demonstrate that our proposed electrochemical biosensor, which integrates with the nicking endonuclease-assisted PER cascade amplification strategy and DNS-mediated electrochemical signal-enhanced system, has been fabricated successfully and possesses high amplification efficiency and sensitivity for miR-21 detection.

Analytical Performance of the Electrochemical Biosensor. The sensitivity and dynamic range of the proposed electrochemical biosensor for miR-21 quantitative detection are evaluated by monitoring the DPV responses to various concentrations of target miRNA. As shown in Figure 4A, a very weak peak current was observed without the target, whereas the DPV intensity enhanced sharply in the presence of the target and continuously increased with the increase in miR-21 concentration from 1 aM to 0.1 nM. In addition, a good linearity between the peak currents and the logarithmic value of miR-21 concentration was obtained (Figure 4B). The detection limit was calculated to be 0.58 aM based on the 3σ/slope method, which is competitive with or even superior to previously reported nuclease-assisted target cascade amplification strategies for miRNA detection (Table S2). Moreover, a control experiment using only the endonuclease-assisted target amplification (cycle I) and only the PER cascades (cycle II) for electrochemical detection of miR-21 with different concentrations was also conducted. The corresponding detection limits were 6.91 aM (S/N = 3) and 4.20 aM (S/N = 3), which were about 11- and 7-fold higher than that of the nuclease-assisted target cascade amplification strategy (cycle I + cycle II), respectively (Figures S6 and S7). Thus, the proposed target cascade amplification strategy possesses a significant contribution to electrochemical signal amplification and the detection sensitivity improvement. The ultrahigh sensitivity of this strategy can be attributed to the following design. (1) The involved DNA probes are totally enclosed and can be activated only by the target miRNA, which effectively prevents the nonspecific leakage from triggering rapid nicking endonu-

https://doi.org/10.1021/acs.analchem.2c03015
Anal. Chem. 2022, 94, 14349−14357

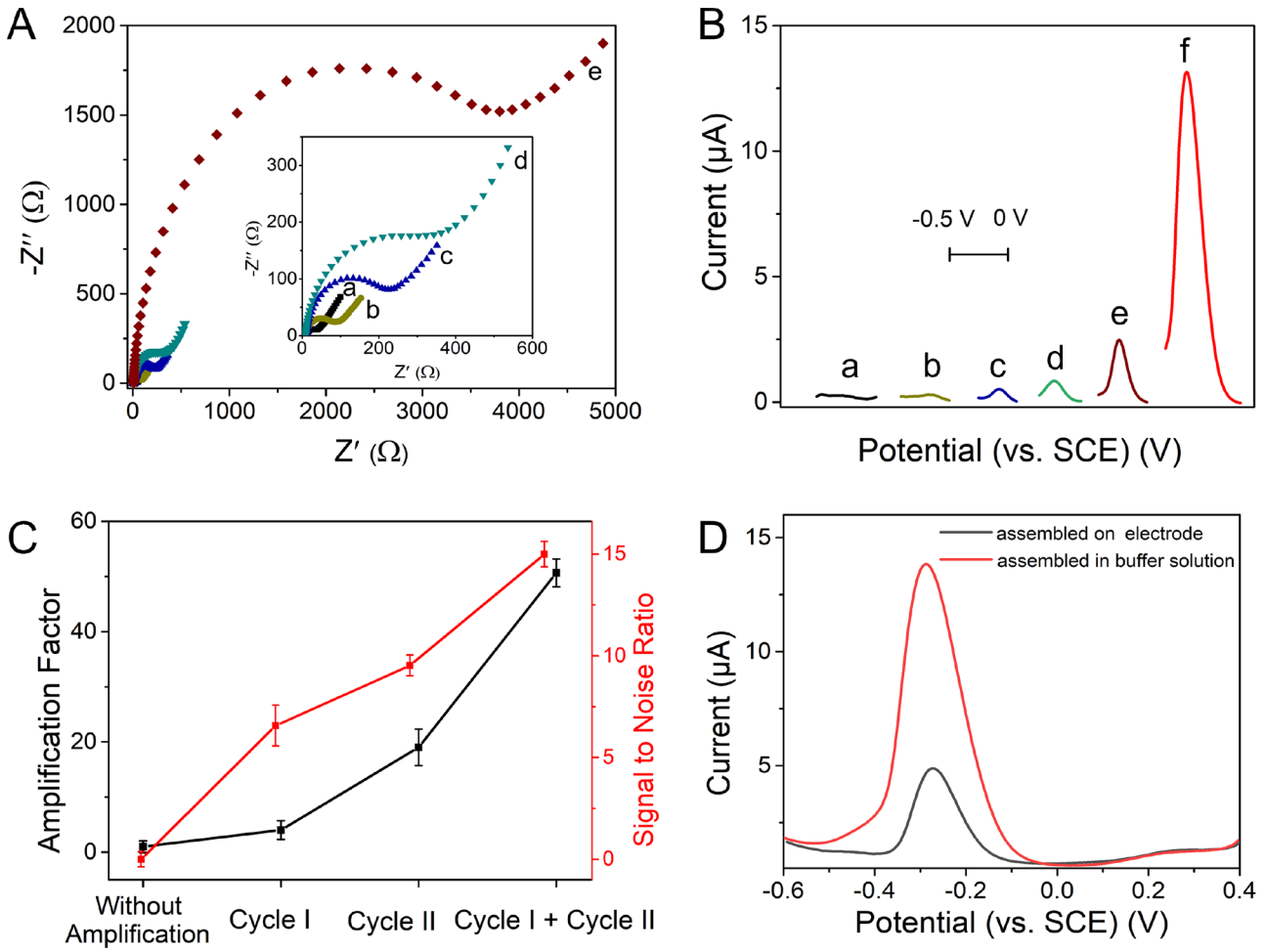

Figure 3. (A) EIS characterization of the step-by-step assembly procedures of the working electrode: (a) bare gold electrode; (b) Cp DNA-modified gold electrode; (c) MCH blocking Cp DNA-modified gold electrode; (d) gold electrode captured the cDNA obtained from nicking endonuclease-assisted PER cascade amplification triggered by miR-21 (1 fM); (e) gold electrode further immobilized with DNS by cDNA (miR-21, 1 fM). (B) DPV curves of different modified gold electrodes: (a) bare gold electrode; (b) Cp DNA-modified gold electrode; (c) gold electrode captured the cDNA obtained from cycle I; (d) gold electrode captured the cDNA obtained from cycle II; (e) gold electrode captured the cDNA obtained from cycle I + cycle II; (f) RuHex-DNS immobilized on the gold electrode by cDNA obtained from cycle I + cycle II. The concentration of miR-21 is 1 fM. (C) Signal-to-noise ratio (the red line) and amplification factors (the black line) of cycle I, cycle II, and cycle I + cycle II. (D) DPV curves of the RuHex-DNS assembled on the gold electrode with two different methods (miR-21, 10 fM).

clease-assisted PER cascade amplification and thus dramatically reduces the background response. (2) The DNS with abundant anionic phosphate can load large amounts of RuHex on the limited working electrode interface, thus achieving a significant enhancement of the electrochemical signal and sensitivity.

The selectivity of this electrochemical platform is further investigated by recording the peak currents of miR-21, microRNA-141 (miR-141), microRNA-125b (miR-125b), one base- and three base-mismatched miR-21 in the same concentration (10 fM). As shown in Figure 4C and Figure S8, compared with the DPV response of miR-21 (f), the DPV responses of other miRNAs (b−e) looked similar to that of the blank (a, that is without any miRNAs). Remarkably, this proposed sensing platform could also accurately identify the target miR-21 in the mixture of these interferential miRNAs (g), which indicated that the excellent selectivity and anti-interference ability of this method allow well distinguishing miR-21 from other interferential miRNAs, even one base-mismatched miR-21. In addition, the reproducibility of the biosensor is evaluated by testing miR-21 with five batch-modified electrodes in the same condition. From Figure 4D and Figure S9, the DPV signal intensity of different batch-modified electrodes has no significant changes, indicating the good reproducibility of this biosensor. Moreover, the Cp DNA-immobilized gold electrode still showed excellent reproducibility after being stored at 4 °C for 10 days (Figure S10), demonstrating that the modified electrode can be prepared in batches and stored at 4 °C for further use, thereby simplifying the experimental operations and shortening the preparation time.

Real Sample Analysis. To evaluate the practicality of this proposed biosensor in real sample detection, various known concentrations of miR-21 are spiked into 10% healthy human serum for carrying out the spike-recovery experiment. As shown in Table S3, the recoveries of miR-21 were in the range of 97.35 to 104.6% with a relative standard deviation (RSD) between 3.60 and 4.44%, indicating that this method has acceptable accuracy for target miRNA detection in the complex sample. Furthermore, this electrochemical biosensor is applied to the analysis of miR-21 derived from different cancer cell lysates, including MCF-7 cells (breast cancer cell

https://doi.org/10.1021/acs.analchem.2c03015
Anal. Chem. 2022, 94, 14349−14357

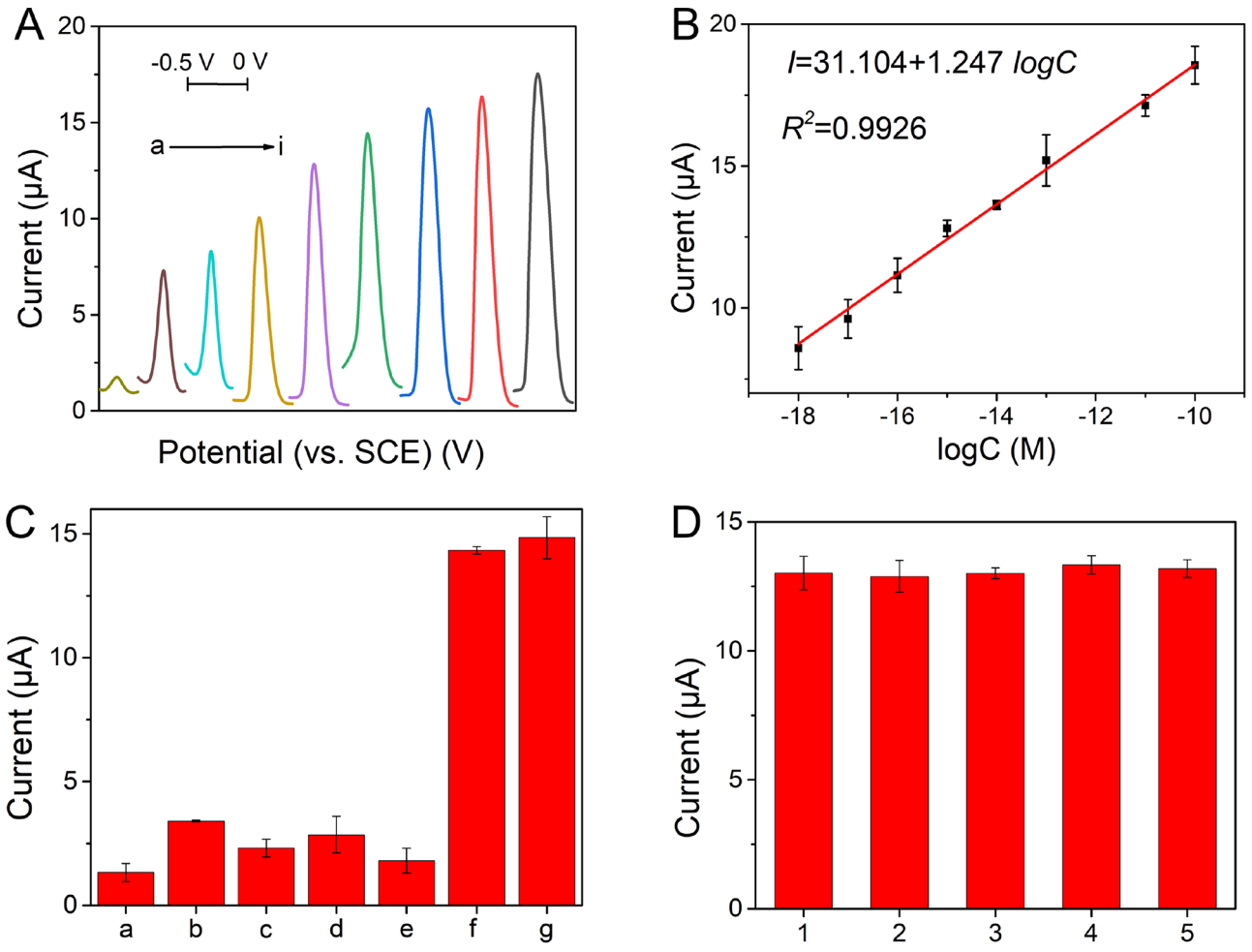

Figure 4. (A) DPV curves of this biosensor in the presence of miR-21 at different concentrations. From panels (a) to (i): 0 aM, 1 aM, 10 aM, 0.1 fM, 1 fM, 10 fM, 0.1 pM, 10 pM, and 0.1 nM. (B) Corresponding calibration curve of peak currents versus the logarithm of miR-21 concentrations. (C) Selectivity of the biosensing platform toward the (a) blank, (b) miR-141, (c) miR-25b, (d) one base-mismatched miR-21, (e) three base-mismatched miR-21, (f) miR-21, and (g) the mixture of these five kinds of miRNAs. (D) DPV response of five batch-modified electrodes in the same condition. The concentration of miR-21 is 1 fM. Error bars represent standard deviations from three repeated measurements.

lines) and HeLa cells (cervical cancer cells). From Figure 5, the peak current intensity obviously increased with increasing MCF-7 cell and HeLa cell numbers from 10^2 to 10^4 and exhibited apparent differences compared to the blank one. Remarkably, the electrochemical signal intensity of cell lysates from MCF-7 cells was higher than that from HeLa cells, which is consistent with a previous report.[44] All of these results demonstrate that the proposed biosensor possesses high practicality in real sample detection, which provides a potential analytical tool for the clinical diagnosis of miRNA-related disease.

CONCLUSIONS

In summary, we have established a nicking endonuclease-assisted PER cascade amplification strategy for electrochemical detection of miR-21 with high sensitivity (detection limit of 0.58 aM) and specificity (one base-mismatch discrimination) as well as excellent reproducibility. The ultrahigh sensitivity originates from the ingenious design. Specifically, the nicking endonuclease-assisted target amplification was combined with the PER cascade for the rapid massive amplification of target miRNA and the improvement of the detection sensitivity. Meanwhile, the DNS-mediated electrochemical signal-en-

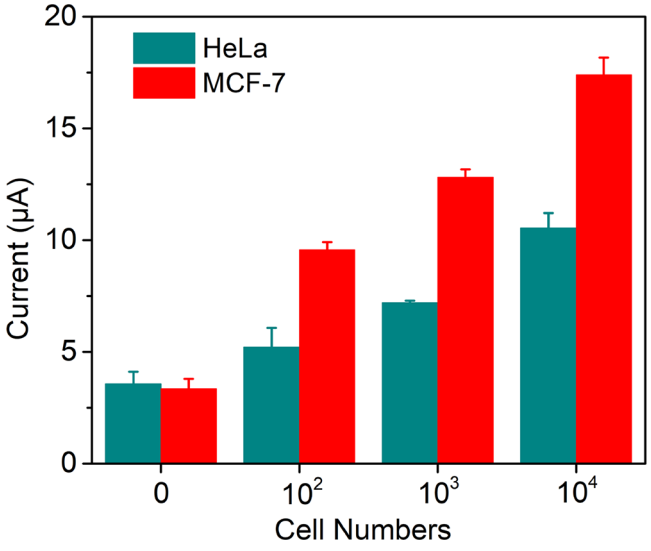

Figure 5. Statistics of miR-21 analysis in MCF-7 cell and HeLa cell lysates. Error bars represent standard deviations from three repeated measurements.

https://doi.org/10.1021/acs.analchem.2c03015
Anal. Chem. 2022, 94, 14349−14357

hanced system breaks through the limitations of the two-dimensional electrode interface, thus achieving an effective improvement of the signal intensity and sensitivity of this electrochemical platform. In addition, the proposed biosensor exhibits a high accuracy and reliability for miR-21 analysis in human serum samples. Furthermore, by detection of miR-21 derived from different cancer cell lysates, the developed strategy has been demonstrated as a powerful tool for specific identification of miR-21-overexpressed cells. Therefore, we believe that this biosensing platform will provide a promising avenue for the detection of valuable biomarkers in early clinical diagnosis and biological applications.

■ ASSOCIATED CONTENT

Supporting Information

The Supporting Information is available free of charge at https://pubs.acs.org/doi/10.1021/acs.analchem.2c03015.

Characterization of DNS; optimization of experimental conditions; stability of the electrochemical signal with different assembly methods; control experiment using only nicking endonuclease-assisted target amplification or PER cascade amplification; influence of the reaction time on different amplification strategies; selectivity and reproducibility of the proposed electrochemical biosensor; comparison of the proposed biosensor with other reports for miRNA detection and the spike-recovery experiments (PDF)

■ AUTHOR INFORMATION

Corresponding Authors

Yuanzhen Zhou − *School of Chemistry and Chemical Engineering, Xi'an University of Architecture and Technology, Xi'an 710055, P. R. China;* orcid.org/0000-0002-9774-1029; Email: zhouyuanzhen@xauat.edu.cn

Jun-Jie Zhu − *School of Chemistry and Chemical Engineering, Xi'an University of Architecture and Technology, Xi'an 710055, P. R. China; State Key Laboratory of Analytical Chemistry for Life Science, School of Chemistry and Chemical Engineering, Nanjing University, Nanjing 210023, P. R. China;* orcid.org/0000-0002-8201-1285; Email: jjzhu@nju.edu.cn

Authors

Sha Yu − *School of Chemistry and Chemical Engineering, Xi'an University of Architecture and Technology, Xi'an 710055, P. R. China;* orcid.org/0000-0003-4121-3814

Siyu Chen − *School of Chemistry and Chemical Engineering, Xi'an University of Architecture and Technology, Xi'an 710055, P. R. China*

Yuan Dang − *School of Chemistry and Chemical Engineering, Xi'an University of Architecture and Technology, Xi'an 710055, P. R. China*

Complete contact information is available at: https://pubs.acs.org/10.1021/acs.analchem.2c03015

Author Contributions

§S.Y. and S.C. contributed equally to this work. S.Y. and S.C. conceived and designed the experiments and performed all experimental work. Y.D. and S.C. analyzed the data. S.Y. and S.C. wrote the original draft. Y.Z. and J.-J.Z. revised the draft elaborately. All authors discussed the results and commented on the manuscript.

Notes

The authors declare no competing financial interest.

■ ACKNOWLEDGMENTS

We gratefully acknowledge the financial support from the Young Scientists Fund of the National Natural Science Foundation of China (22104118). We also thank the financial support from State Key Laboratory of Analytical Chemistry for Life Science (SKLACLS2204), the Natural Science Foundation of Shaanxi Province (2020JM-480), and the Key Scientific Research Project of Shaanxi Provincial Department of Education (20JS074).

■ REFERENCES

(1) He, L.; Hannon, G. J. *Nature* **2004**, *5*, 522−531.
(2) Bartel, D. P. *Cell* **2004**, *116*, 281−297.
(3) Brennecke, J.; Hipfner, D. R.; Stark, A.; Russell, R. B.; Cohen, S. M. *Cell* **2003**, *113*, 25−36.
(4) Xu, P.; Wu, Q.; Yu, J.; Rao, Y.; Kou, Z.; Fang, G.; Shi, X.; Liu, W.; Han, H. *Front. Genet.* **2020**, *11*, 278−290.
(5) Fuentes, E.; Palomo, I.; Alarcon, M. *Life Sci.* **2015**, *133*, 29−44.
(6) Wang, H. *Biomedicines* **2020**, *8*, 530−546.
(7) Alwine, J. C.; Kemp, D. J.; Stark, G. R. *Proc. Natl. Acad. Sci. U. S. A.* **1977**, *74*, 5350−5354.
(8) Wang, S.-T.; Li, C.; Liu, L. *Curr. Bioinf.* **2009**, *4*, 141−148.
(9) Harshitha, R.; Arunraj, D. R. *Biochem. Mol. Biol. Educ.* **2021**, *49*, 800−812.
(10) Qavi, A. J.; Kindt, J. T.; Bailey, R. C. *Anal. Bioanal. Chem.* **2010**, *398*, 2535−2549.
(11) Planell-Saguer, M.; Rodicio, M. C. *Anal. Chim. Acta* **2011**, *699*, 134−152.
(12) Wu, Y.; Fu, C.; Shi, W.; Chen, J. *Talanta* **2021**, *235*, 122735−122756.
(13) Li, D.; Zhang, T.; Yang, F.; Yuan, R.; Xiang, Y. *Anal. Chem.* **2020**, *92*, 2074−2079.
(14) Connolly, A. R.; Trau, M. *Angew. Chem., Int. Ed.* **2010**, *49*, 2720−2723.
(15) Kumar, Y.; Bansal, S.; Jaiswal, P. *Compr. Rev. Food Sci. Food Saf.* **2017**, *16*, 1359−1378.
(16) Qian, C.; Wang, R.; Wu, H.; Ji, F.; Wu, J. *Anal. Chim. Acta* **2019**, *1050*, 1−15.
(17) Gill, P.; Ghaemi, A. *Nucleosides, Nucleotides Nucleic Acids* **2008**, *27*, 224−243.
(18) Gines, G.; Menezes, R.; Xiao, W.; Rondelez, Y.; Taly, V. *Mol. Aspects. Med.* **2020**, *72*, 100832−100849.
(19) Kishi, J. Y.; Lapan, S. W.; Beliveau, B. J.; West, E. R.; Zhu, A.; Sasaki, H. M.; Saka, S. K.; Wang, Y.; Cepko, C. L.; Yin, P. *Nat. Methods* **2019**, *16*, 533−544.
(20) Zhang, J.; He, M.; Nie, C.; He, M.; Pan, Q.; Liu, C.; Hu, Y.; Chen, T.; Chu, X. *Chem. Sci.* **2020**, *11*, 7092−7101.
(21) Kishi, J. Y.; Schaus, T. E.; Gopalkrishnan, N.; Xuan, F.; Yin, P. *Nat. Chem.* **2018**, *10*, 155−164.
(22) Tavakoli-Koopaei, R.; Javadi-Zarnaghi, F.; Mirhendi, H. *Sens. Actuators B* **2022**, *357*, 131409−131419.
(23) Zhou, W.; Xu, L.; Jiang, B. *Anal. Chim. Acta* **2021**, *1148*, 238195−238201.
(24) Li, X.; Li, X.; Li, D.; Zhao, M.; Wu, H.; Shen, B.; Liu, P.; Ding, S. *Biosens. Bioelectron.* **2020**, *168*, 112554−112560.
(25) Yu, S.; Wang, Y.; Jiang, L.-P.; Bi, S.; Zhu, J.-J. *Anal. Chem.* **2018**, *90*, 4544−4551.
(26) Maduraiveeran, G.; Sasidharan, M.; Ganesan, V. *Biosens. Bioelectron.* **2018**, *103*, 113−129.
(27) Lu, J.; Wang, M.; Han, Y.; Deng, Y.; Zeng, Y.; Li, C.; Yang, J.; Li, G. *Anal. Chem.* **2022**, *94*, 5055−5061.
(28) Chang, J.; Wang, X.; Wang, J.; Li, H.; Li, F. *Anal. Chem.* **2019**, *91*, 3604−3610.

(29) Liu, J.; Kong, D.; Liu, Z.; Liu, H.; Yi, J.; Tian, D.; Xia, F.; Zhou, C. *Sens. Actuators B* **2020**, *319*, 128246−128252.
(30) Wang, D.-X.; Wang, J.; Wang, Y.-X.; Du, Y.-C.; Huang, Y.; Tang, A.-N.; Cui, Y.-X.; Kong, D.-M. *Chem. Sci.* **2021**, *12*, 7602−7622.
(31) Yu, S.; Wang, Y.; Li, Y.; Jiang, L.-P.; Bi, S.; Zhu, J.-J. *Adv. Funct. Mater.* **2019**, *29*, 1905659.
(32) Li, Y.; Mao, C.; Deng, Z. *Chin. J. Chem.* **2017**, *35*, 801−810.
(33) Liu, L.; Han, L.; Wu, Q.; Sun, Y.; Li, K.; Liu, Y.; Liu, H.; Luo, E. *J. Mater. Chem. B* **2021**, *9*, 4991−5007.
(34) Lv, J.; Dong, Y.; Gu, Z.; Yang, D. *Chem. − Eur. J.* **2020**, *26*, 14512−14524.
(35) Yue, S.; Qiao, Z.; Yu, K.; Hai, X.; Li, Y.; Li, Y.; Song, W.; Bi, S. *Chem. Eng. J.* **2021**, *408*, 127258−127267.
(36) Liu, P.; Qian, X.; Li, X.; Fan, L.; Li, X.; Cui, D.; Yan, Y. *ACS Appl. Mater. Interfaces* **2020**, *12*, 45648−45656.
(37) Cai, R.; Zhang, S.; Chen, L.; Li, M.; Zhang, Y.; Zhou, N. *ACS Appl. Mater. Interfaces* **2021**, *13*, 4905−4914.
(38) Kangkamano, T.; Numnuam, A.; Limbut, W.; Kanatharana, P.; Vilaivan, T.; Thavarungkul, P. *Biosens. Bioelectron.* **2018**, *102*, 217−225.
(39) Cheng, H.; Li, W.; Duan, S.; Peng, J.; Liu, J.; Ma, W.; Wang, H.; He, X.; Wang, K. *Anal. Chem.* **2019**, *91*, 10672−10678.
(40) Wang, W.-J.; Li, J.-J.; Rui, K.; Gai, P.-P.; Zhang, J.-R.; Zhu, J.-J. *Anal. Chem.* **2015**, *87*, 3019−3026.
(41) Wang, Y.; Jiang, L.-P.; Zhou, S.; Bi, S.; Zhu, J.-J. *ACS Appl. Mater. Interfaces* **2016**, *8*, 26532−26540.
(42) Zhu, L.; Zhang, M.; Ye, J.; Yan, M.; Zhu, Q.; Huang, J.; Yang, X. *Anal. Chem.* **2020**, *92*, 8614−8622.
(43) Zhang, Y.; Zhang, X.; Situ, B.; Wu, Y.; Luo, S.; Zheng, L.; Qiu, Y. *Biosens. Bioelectron.* **2021**, *183*, 113205.
(44) Bao, T.; Fu, R.; Jiang, Y.; Wen, W.; Zhang, X.; Wang, S. *Anal. Chem.* **2021**, *93*, 13475−13484.

Recommended by ACS

Zinc-Air Battery-Based Self-Powered Sensor with High Output Power for Ultrasensitive MicroRNA let-7a Detection in Cancer Cells

Yunxia Jin, Shengfu Wang, *et al.*
OCTOBER 05, 2022
ANALYTICAL CHEMISTRY
READ

DNA Zipper Mediated Membrane Fusion for Rapid Exosomal MiRNA Detection

Miao Xie, Chuan Zhang, *et al.*
SEPTEMBER 16, 2022
ANALYTICAL CHEMISTRY
READ

Versatile Electrochemical Biosensor Based on the Target-Controlled Capture and Release of DNA Nanotubes for the Ultrasensitive Detection of Multiplexed Biomarkers

Lingqi Kong, Ruo Yuan, *et al.*
AUGUST 05, 2022
ANALYTICAL CHEMISTRY
READ

Smart Programmable Scalable Dual-Mode Diagnostic Logic Nanoflare Strategy for Dual-Tumor Marker Detection

Zhiheng Cai, Fenglei Gao, *et al.*
JUNE 30, 2022
ANALYTICAL CHEMISTRY
READ

Get More Suggestions >

https://doi.org/10.1021/acs.analchem.2c03015
Anal. Chem. 2022, 94, 14349−14357